Journal of Alloys and Compounds 527 (2012) 16–24

Contents lists available at SciVerse ScienceDirect

Journal of Alloys and Compounds

journal homepage: www.elsevier.com/locate/jallcom

A structural review of nanoscopic $Al_{1-x}TM_x$ phase formation in the $TMCl_n$ enhanced $NaAlH_4$ system

M.P. Pitt[a,c,e,*], P.E. Vullum[b], M.H. Sørby[a], H. Emerich[d], M. Paskevicius[c], C.E. Buckley[c], E. MacA. Gray[e], J.C. Walmsley[b,f], R. Holmestad[b], B.C. Hauback[a]

[a] Physics Department, Institute for Energy Technology, P.O. Box 40, Kjeller N-2027, Norway
[b] Department of Physics, Norwegian University of Science and Technology, N-7491 Trondheim, Norway
[c] Department of Imaging and Applied Physics, Curtin University, GPO Box U1987, Perth 6845, Western Australia, Australia
[d] Swiss-Norwegian Beam Line, European Synchrotron Radiation Facility, BP 220 Grenoble CEDEX, France
[e] Queensland Micro and Nanotechnology Centre, Griffith University, Brisbane 4111, Australia
[f] SINTEF, Materials and Chemistry, NO-7465 Trondheim, Norway

ARTICLE INFO

Article history:
Received 16 December 2011
Received in revised form 6 February 2012
Accepted 6 February 2012
Available online xxx

Keywords:
Metal hydrides
Transition metal alloys and compounds
Synchrotron radiation

ABSTRACT

The twice hydrogen (H) cycled planetary milled (PM) $NaAlH_4 + xTMCl_n$ (transition metal (TM) = Sc, Ti, V, Cr, Mn, Fe, Co, Ni, Cu, Zr, Pd, Pt; $2 < n < 4$) and cryo milled (CM) $NaAlH_4 + xTMCl_n$ (TM = Ti, V, Cr, Fe, Ni; $2 < n < 3$) systems ($x < 0.1$) have been studied by high resolution synchrotron X-ray diffraction. Face centred cubic (fcc) A1 crystalline (c-) $Al_{1-x}TM_x$ ($x < 0.25$) solid solutions are evident in PM samples for Sc, Ti, V, Cr, Mn, Zr and Pd while PM samples of Cu, Ni, Pd and Pt display mostly ordered and numerous crystalline $Al_{1-x}TM_x$ phases. Very broad reflections in the 2 Å d-spacing region for Cr, Mn, Co, and Pd are identified as partially ordered body centred cubic (bcc) A2 and B2 $Al_{1-x}TM_x$ type structures. The amorphous (a-) $Al_{1-x}V_x$ phase observed in the H cycled PM $NaAlH_4 + xVCl_3$ system ranges in composition from a-$Al_{90}V_{10}$ ($x = 0.02$) up to a-$Al_{72}V_{28}$ ($x = 0.1$). Across the TM series, the $Al_{1-x}TM_x$ particle size ranges as Sc-V 4-25 nm, Cr, Mn, Co <5 nm, Fe 5–15 nm, Ni, Cu <50 nm. A highly 'compressed' $NaAlH_4$ phase is observed in the H cycled PM $NaAlH_4 + 0.1ScCl_3$ system, with unit cell dimensions of $a = 4.9995(2)$ Å and $c = 11.2893(1)$ Å, compared to the average dimensions of 'normal' $NaAlH_4$ across the TM and rare earth (RE) series with $a = 5.0228(1)$ Å and $c = 11.3516(1)$ Å.

1. Introduction

While the Ti enhanced $NaAlH_4$ system remains the prototypical hydrogen storage material in the 'complex' hydride family, several other catalytic metal species have been identified that produce hydrogenation kinetics that are at least as rapid as Ti-based additives, in particular $ScCl_3$ [1–4] and $CeCl_3$ [1,3,5–7]. The review of desorption kinetics for $TMCl_n$ enhanced $NaAlH_4$ in [8] shows that a wide variety of transition metal and rare earth (RE) atoms (almost all are added as metal-chlorides) can be of minor to major benefit to $NaAlH_4$ in terms of improving de-hydrogenation kinetics, including Ag, Cd, Ce, Co, Cr, Cu, Fe, Ga, Gd, Hf, Mn, Mo, Nb, Pd, Pt, Rh, Ru, Sr, V, Yb, Zn, and Zr. Every one of these atoms allowed at least partial hydrogen desorption to occur below the $NaAlH_4$ melting temperature when the metal-chloride was co-milled with $NaAlH_4$. Other metal-chlorides of interest that have been added to $NaAlH_4$ with catalytic benefit include $PrCl_3$ [1], and $ErCl_3$, $LaCl_3$, $NdCl_3$ and $SmCl_3$ [9].

While it is clear for the $TiCl_3$ enhanced $NaAlH_4$ system that a range of $Al_{1-x}Ti_x$ compositions can form depending on $TiCl_3$ content, milling and hydrogen cycling conditions [10,11], structural studies of the reduction mechanisms of the above wide range of metal-chloride additives with $NaAlH_4$ are surprisingly limited. Al_3Sc, ScH_2 and an $Al_{1-x}Sc_x$ solid solution of unidentified composition are reported from solid state ^{45}Sc nuclear magnetic resonance (NMR) data for milled and H cycled $NaAlH_4 + 0.06ScCl_3$ [4]. Low angle shoulders on Al reflections are observed in laboratory source diffraction data for thermally desorbed (to 400 °C) $NaAlH_4 + 0.04ScCl_3$ [12], where the formation of $Al_{1-x}Sc_x$ solid solution is proposed, but no analysis or phase composition is reported. Al_4Ce is observed in milled and H cycled $NaH + Al + 0.02CeCl_3$ in [6], and disordered AlCe and a new form of bcc Al_2Ce are observed in milled and H cycled $NaH + Al + 0.02CeCl_3$ respectively in [7]. As shown for $TiCl_3$ [10,11], it appears that the type of $Al_{1-x}Ce_x$ phase observed is dependent on milling and H cycling conditions for $CeCl_3$ enhanced $NaAlH_4$. A La_3Al_{11} composition is reported for $LaCl_3$ enhanced $NaAlH_4$ in [9]. Al_3V and Al_3Hf are suggested to form for PM $NaAlH_4 + 0.04VCl_3$ and PM $NaAlH_4 + 0.04HfCl_4$ [13]. $Al_{1-x}Zr_x$

* Corresponding author at: Hydrogen Storage Research Group, Department of Imaging and Applied Physics, Curtin University, Kent Street, Bentley, Perth 6102, Western Australia, Australia. Tel.: +61 8 9266 3673; fax: +61 8 9266 2377.
E-mail address: mark.pitt@gmail.com (M.P. Pitt).

0925-8388/$ – see front matter © 2012 Elsevier B.V. All rights reserved.
doi:10.1016/j.jallcom.2012.02.055

compositions of $Al_{3.93}Zr_{0.07}$ to $Al_{3.2}Zr_{0.8}$ (mol% $ZrCl_4$ dependent) for rehydrogenated PM $NaAlH_4$ + 0.04–0.25$ZrCl_4$ are discussed in [14].

A common theme among these reported works is the formation of $Al_{1-x}TM_x$ or $Al_{1-x}RE_x$ phases (including disordered, ordered and solid solution phases) upon the addition of $TMCl_n$ and $RECl_n$ to $NaAlH_4$. As shown in our previous studies of $TiCl_3$ enhanced $NaAlH_4$, the formation of isolated nanoscopic $Al_{1-x}Ti_x$ phases on the $NaAlH_4$ surface [15] is crucial for hydrogen uptake and release [16]. In this study, we utilise the 1st row of transition metals (and selected 2nd and 3rd row elements), and observe by high resolution synchrotron X-ray diffraction which $Al_{1-x}TM_x$ phases form from the addition of $TMCl_n$ additives to $NaAlH_4$.

2. Experimental procedure

$NaAlH_4$ was purchased from Albemarle Corporation (LOT NO.#: 22470404-01, >93% purity). All transition-metal-chloride precursors were purchased from Sigma–Aldrich Chemicals Inc. (typically >99.99% purity). At all times, all powders have been handled under inert Ar atmosphere in a dry glove box, with <1 ppm O_2 and H_2O. Milled $NaAlH_4$ + $x TMCl_n$ powders were prepared in 1 g quantities in a Fritsch P7 planetary mill, with ball to powder ratio (bpr) of 20:1, at 750 rpm for a period of 1 h, and in 2 g quantities in a Spex 6750 Freezer mill, milled at intensity 15 for a period of 2 h, in a custom sealed stainless steel cryo vial, with a 32 g AISI440c impactor. Milling was performed under Ar from the glove box. Hydrogen cycling was performed in a Sieverts apparatus composed of commercial VCR components, rated to 200 bar and 600 °C. Hydrogen compressibility was modeled with the most accurate known equation of state [17], and a divided volume model was applied to accurately account for the total amount of hydrogen in the system in the presence of a temperature distribution [18]. Hydrogen cycling conditions were: absorption at 140 °C under 150 bar system pressure, and desorption at 140 °C under ultra high vacuum (<10^{-6} mbar). Both H absorption and desorption were carried out over 12 h time periods. Powders were studied typically after 2 H cycles for diffraction measurements, typically in the H full state. Powder X-ray diffraction data was recorded at the Swiss-Norwegian Beamline (SNBL) at the European Synchrotron Radiation Facility (ESRF) in Grenoble, France. Samples were contained in rotating 0.8 mm boron-silica glass capillaries. High resolution data ($\Delta d/d \sim 3 \times 10^{-4}$) was typically collected at 295 K between 5° and 35° 2θ, in steps of 0.003–0.030°, depending on the sample broadening. A wavelength of 0.4998 Å was obtained from a channel cut Si(1 1 1) monochromator. Synchrotron X-ray diffraction patterns were analysed by the Rietveld method using RIETICA [19]. Diffraction lineshape profiles were fitted with a full Voigt function, with the instrumental shape determined by a NIST LaB_6 660a lineshape standard, further annealed to 1800 °C. All measured $NaAlH_4$ and $Al_{1-x}TM_x$ unit cell dimensions quoted below possess an average uncertainty within ±0.0003 Å, which is quoted in parentheses for the last decimal place.

3. Results and discussion

Fig. 1 presents a series of synchrotron X-ray diffraction patterns for the twice H cycled $NaAlH_4$ + 0.1$TMCl_n$ samples TM = Sc, Ti, V, Cr, Mn, Fe, and Co, across the most interesting d-spacing range from 1.9 to 2.4 Å. The data are scaled to match the (1 1 1) NaCl intensity contribution. Very broad peaks are evident for Cr, Mn and Co, with peak maximas occurring in the 2.04–2.21 Å range. The broad peaks indicate either nanoscopic or amorphous $Al_{1-x}TM_x$ phases, dependent on the observation of further broad crystalline reflections at lower d-spacings. As discussed in [20], the broad peaks from PM and H cycled VCl_3 and $FeCl_3$ enhanced $NaAlH_4$ are the primary halo from amorphous a-$Al_{72}V_{28}$, and a-$Al_{88.5}Fe_{11.5}$ respectively. For the H cycled PM $NaAlH_4$ + 0.1VCl_3 system, we observe both crystalline and amorphous $Al_{1-x}V_x$ phases co-exisiting in a composite nanoscopic morphology embedded on the $NaAlH_4$ surface. A c-$Al_{90}V_{10}$ solid solution (producing the low d-spacing shoulders on Al reflections in Fig. 1) is embedded within the a-$Al_{72}V_{28}$ matrix [20]. In the discussion below, we describe how the broad peaks from Cr, Mn and Co are not primary halos from amorphous phases, rather, they represent extremely broad reflections from nanoscopic bcc $Al_{1-x}TM_x$ solid solutions.

Across the TM series, we observe a range of crystalline $Al_{1-x}TM_x$ solid solution phases. Fig. 2 shows the (1 1 1) reflection of crystalline fcc $Al_{1-x}TM_x$ ($x < 0.25$) solid solutions formed for TM = Sc, Ti, V, Cr, Mn, Zr and Pd in twice H cycled PM $NaAlH_4$ + 0.1$TMCl_n$, with their associated unit cell dimension. We observe crystalline fcc solid solutions that typically contain significantly more TM atoms than the maximum TM solubility according to the equilibrium phase diagram, such as $Al_{87.6}Sc_{12.4}$ (see analysis below), with equilibrium solubility of 0.08 at.% Sc [21], $Al_{85}Ti_{15}$ [10] (equilibrium solubility of 2 at.% [22]), $Al_{90}V_{10}$ [20] (equilibrium solubility of 0.2 at.% [23]), $Al_{97.73}Cr_{2.27}$ [24] (equilibrium solubility of 0.04 at.% [25]), $Al_{95.67}Mn_{4.33}$ [26] (equilibrium solubility of 0.65 at.% [27]), $Al_{94.5}Zr_{5.5}$ [28] (equilibrium solubility of 0.08 at.% [28]), and $Al_{90}Pd_{10}$ [29] (equilibrium solubility of 0.2 at.% [30]). For fcc $Al_{1-x}TM_x$ solid solutions with extended solubility, knowledge of the concentration dependent ($0 < x < 25$ at.%) lattice parameters is crucial to determine the correct Al:TM composition, as discussed extensively for the Ti case in [10], and for the concentration dependent lattice parameters provided for Cr, Mn and Zr in [24,26,28] respectively. All fcc $Al_{1-x}TM_x$ solid solution compositions are summarised in Tables 1 and 2.

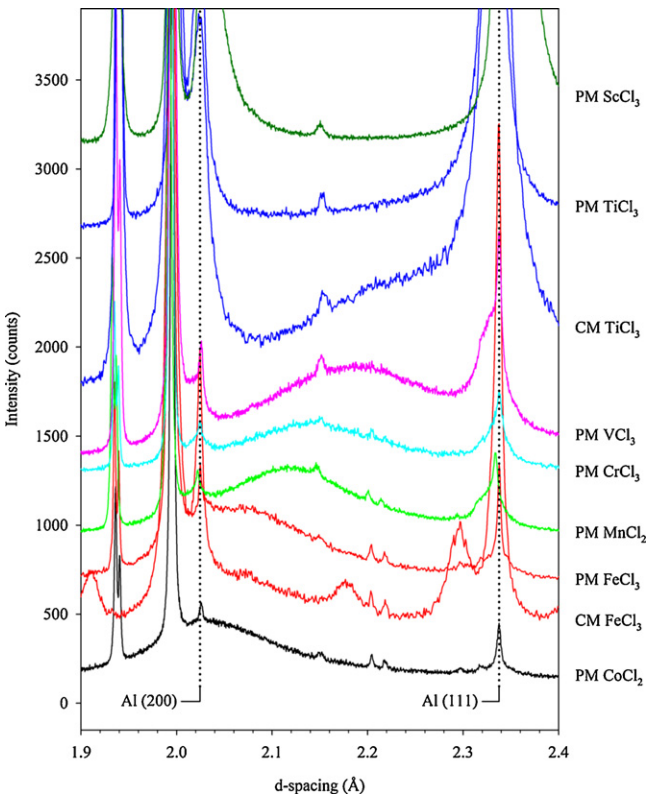

Fig. 1. Raw data series from 1.9 to 2.4 Å for the twice H cycled $NaAlH_4$ + 0.1$TMCl_n$ samples TM = Sc, Ti, V, Cr, Mn, Fe, and Co. The maxima of primary amorphous $Al_{1-x}TM_x$ halos are evident for Ti based samples at ca. 2.21 Å, for V based samples at ca. 2.19 Å, and for Fe based samples at ca. 2.06 Å. PM = planetary milled, CM = cryogenically milled.

To date, we have not found accurate concentration dependent lattice parameters for c-$Al_{1-x}Sc_x$ ($x < 0.25$) solid solution beyond 3.2 at.% Sc [31]. The $Al_{1-x}Sc_x$ phase in our twice H cycled PM $NaAlH_4$ + 0.02–0.1$ScCl_3$ samples possess a unit cell dimension of 4.0802(1) Å, below the 4.1030 Å unit cell reported for the ordered $L1_2$ Al_3Sc phase [32]. A unit cell of 4.0650 Å is reported for the solid solution $Al_{96.8}Sc_{3.2}$ [31]. On the basis of a 4.0802(1) Å unit cell dimension, we expect the $Al_{1-x}Sc_x$ composition to lie in the range $0.032 < x < 0.25$. The $NaAlH_4$ + 0.02$ScCl_3$ sample appears kinetically very similar to the $NaAlH_4$ + 0.02$TiCl_3$ sample, showing absorption kinetics of 25.78 wt.% H/h and 22.67 wt.% H/h, respectively. The diffraction patterns for twice H cycled $NaAlH_4$ + 0.02$TMCl_3$ (TM = Sc, Ti) are also very similar, with the only observable

Table 1
$Al_{1-x}TM_x$ phases determined for the twice H cycled PM $NaAlH_4$ + 0.1$TMCl_n$ system. The percentage of TM atoms in each phase is denoted below each phase.

$ScCl_3$	VCl_3	$CrCl_3$	$MnCl_2$	$FeCl_3$	$CoCl_2$	$NiCl_2$	$CuCl_2$	$ZrCl_4$	$PdCl_2$	$PtCl_4$	$YbCl_3$
$Al_{87.6}Sc_{12.4}$ (70.33%) (PM 2 mol%) ×2 H cycle $Al_{87.6}Sc_{12.4}$ (79.16%) (PM 10 mol%) ×2 H cycle	c-$Al_{90}V_{10}$ (14.73%) a-$Al_{90}V_{10}$ (85.27%) (by QPA) (PM 2 mol%) ×2 H cycle c-$Al_{90}V_{10}$ (13.54%) a-$Al_{72}V_{28}$ (86.46%) (by QPA) a-$Al_{70}V_{30}$ (by EDS) (PM 10 mol%) ×2 H cycle [18] a-$Al_{83}V_{17}$ (100%) CM 10 mol%) ×2 H cycle	$Al_{97.73}Cr_{2.27}$ (0.64%) $Al_{48.2}Cr_{51.8}$ (99.36%) (PM 10 mol%) ×10 H cycle	$Al_{95.67}Mn_{4.33}$ (0.31%) $Al_{65.5}Mn_{34.5}$ (99.69%) (PM 10 mol%) ×2 H cycle	a-$Al_{88.5}Fe_{11.5}$ (by QPA) a-$Al_{66}Fe_{34}$ (by EDS) (100%) (PM 10 mol%) ×2 H cycle [18] a-$Al_{1-x}Fe_x$ c-Al_2Fe (structure unknown; new phase) (CM 10 mol%) ×2 H cycle	AlCo (100%) (PM 10 mol%) ×2 H cycle	Al_9Ni_2 (17.97%) Al_3Ni (58.02%) Al_4Ni_3 (1.10%) AlNi (19.05%) $Ni_{86}Al_{14}$ (3.86%) (PM, CM 10 mol%) ×2 H cycle	Al_2Cu (70.12%) Cu_3Al (25.36%) Al_3Cu_4 (3.33%) Cu (1.19%) (PM 10 mol%) ×2 H cycle	$Al_{94.5}Zr_{5.5}$ (42.50%) Al_3Zr (56.75%) ZrH_2 (0.75%) (PM 10 mol%) ×2 H cycle	$Al_{90}Pd_{10}$ (16.14%) Al_4Pd (0.09%) Al_3Pd (40.76%) Al_3Pd_2 (0.16%) AlPd (42.40%) Pd (0.45%) (PM 10 mol%) ×2 H cycle	$Al_{21}Pt_8$ (16.16%) Al_4Pt (16.16%) Al_3Pt_2 (17.78%) Al_2Pt (13.54%) Al_3Pt_5 (7.07%) $AlPt_3$ (high T) (10.91%) AlPt (FeSi) (7.68%) AlPt (CsCl) (1.01%) Pt (9.70%) (PM 10 mol%) ×2 H cycle	Al_2Yb (40.95%) YbH_3 (59.05%) (CM 10 mol%) ×2 H cycle

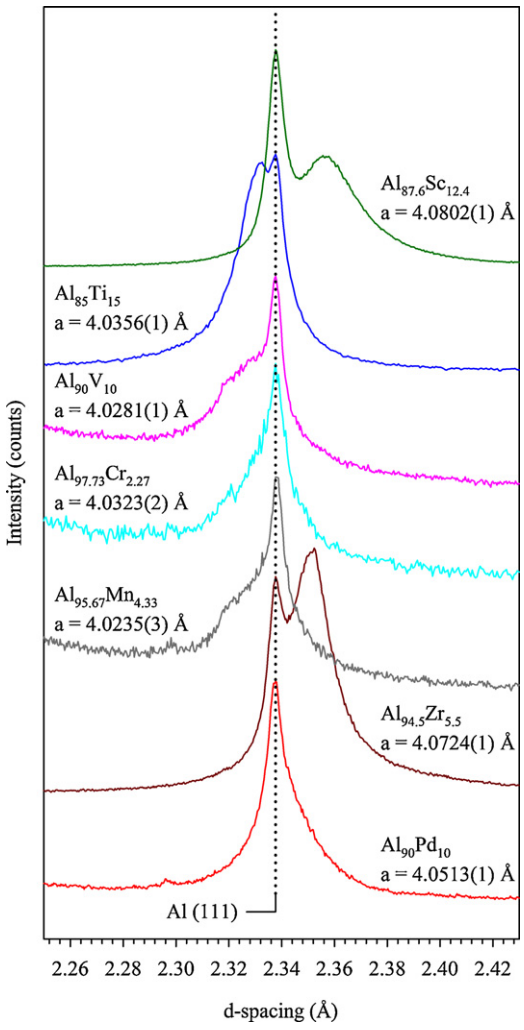

Fig. 2. A mulitplot of twice H cycled PM $NaAlH_4 + 0.1TMCl_n$ samples, showing the fcc c-$Al_{1-x}TM_x$ ($x < 0.25$) solid solutions that have formed for TM = Sc, Ti, V, Cr, Mn, Zr and Pd. Al:TM composition and unit cell dimensions are shown.

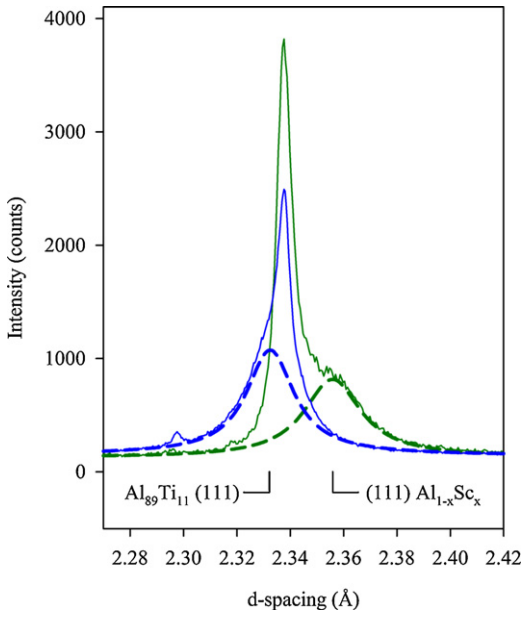

Fig. 3. The relative integrated diffraction intensity of (1 1 1) for $Al_{1-x}TM_x$ ($x < 0.25$) in twice H cycled $NaAlH_4 + 0.02TMCl_3$ (TM = Sc, Ti).

reflections from the TM containing phases being the crystalline $Al_{1-x}TM_x$ solid solution with $x < 0.25$. Fig. 3 compares the (1 1 1) intensity of the known c-$Al_{89}Ti_{11}$ solid solution [11] with the unknown c-$Al_{1-x}Sc_x$ ($x < 0.25$) solid solution (1 1 1) intensity (the data have been scaled so that NaCl intensity is equal). Integrating the (1 1 1), (2 0 0) and (2 2 0) intensities for each c-$Al_{1-x}TM_x$ ($x < 0.25$) phase also demonstrates that the total intensity contribution is very similar, with $I_{111}Al_{89}Ti_{11} = 0.9752I_{111}$ $Al_{1-x}Sc_x$. With X-ray scattering factors that are very close in magnitude for Sc and Ti, and very similar absorption kinetics and diffracted intensity from c-$Al_{1-x}TM_x$ ($x < 0.25$), it is then straightforward to determine the unknown Al:Sc ratio from the known $Al_{89}Ti_{11}$ composition, utilizing I_{111} $Al_{89}Ti_{11} = 0.9752I_{111}$ $Al_{1-x}Sc_x$. This yields a c-$Al_{87.6}Sc_{12.4}$ composition. The concentration dependent unit cell dimension for the c-$Al_{1-x}Sc_x$ ($x < 0.25$) system can been constructed on the basis of our calculated $Al_{87.6}Sc_{12.4}$ composition, and the reported unit cells for $Al_{96.8}Sc_{3.2}$ [31] and $L1_2$ Al_3Sc [32]. The variation of unit cell dimension up to 25 at.% Sc is shown in Fig. 4. The concentration dependence of the unit cell shows a similar variation in the c-$Al_{1-x}Ti_x$ ($x < 0.25$) system [33], except that the $Al_{1-x}Sc_x$ cell expands, and the $Al_{1-x}Ti_x$ cell contracts relative to pure Al. By itself, the c-$Al_{87.6}Sc_{12.4}$ solid solution accounts for 70.33% of the originally added Sc atoms, very similar to the Ti case, where c-$Al_{89}Ti_{11}$ can account for 65.94% of the originally added Ti atoms for the $NaAlH_4 + 0.02TiCl_3$ system [11]. Based on observing Al_2Ti and Al_3Ti in the early H cycles for the $NaAlH_4 + 0.02TiCl_3$ system [11] and the similar absorption kinetics between $ScCl_3$ and $TiCl_3$ enhanced $NaAlH_4$, we also expect that Al_2Sc and Al_3Sc may analogously form in the $NaAlH_4 + 0.02ScCl_3$ system. Al_2Sc and Al_3Sc are known intermetallics in the binary Al–Sc phase diagram [34], and Al_3Sc and a c-$Al_{1-x}Sc_x$ solid solution of unspecified composition have been observed in the $NaAlH_4 + 0.06ScCl_3$ system after eight H cycles by solid state NMR [4]. Al_3Sc precipitation from $Al_{1-x}Sc_x$ ($x < 0.25$) solid solution is also well studied in Al–Sc metallurgy [35], and we expect to always find Al_3Sc and $Al_{1-x}Sc_x$ together in a composite morphology, again similar to the case for $TiCl_3$ enhanced $NaAlH_4$, where Al_3Ti and $Al_{1-x}Ti_x$ ($x < 0.25$) are always observed together

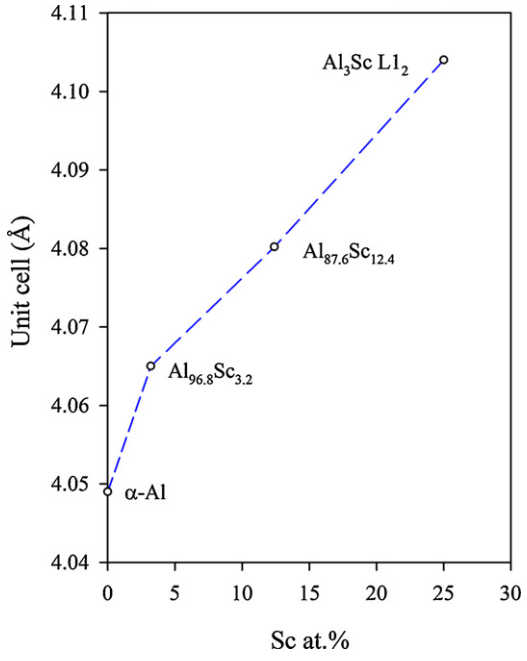

Fig. 4. Variation of the crystalline c-$Al_{1-x}Sc_x$ solid solution unit cell dimension as a function of Sc content in the $0 < x < 25$ at.% Sc range.

[11]. TEM is required to verify the existence of Al_2Sc in the early H cycles for the $NaAlH_4 + 0.02ScCl_3$ system, and to subsequently complete the quantitative phase analysis (QPA) and account for all originally added Sc atoms. We expect that up to ca. 25% of the originally added Sc atoms will be found within the Al_2Sc phase, similar to the $NaAlH_4 + 0.02TiCl_3$ system [11].

At higher $ScCl_3$ additive level, there is a dramatic reduction in absorption kinetics from ca. 25.78 wt.% H/h for 2 mol% $ScCl_3$, down to 0.029 wt.% H/h for 10 mol% $ScCl_3$. Diffraction data from the twice H cycled $NaAlH_4 + 0.1ScCl_3$ system (see Fig. 1) shows an identical c-$Al_{1-x}Sc_x$ solid solution with the same 4.0802(1) Å unit cell dimension as 2 mol% $ScCl_3$ additive level, indicating the same c-$Al_{87.6}Sc_{12.4}$ solid solution is present. However, weak $L1_2$ ordering reflections can be observed for the c-$Al_{87.6}Sc_{12.4}$ solid solution, with $I(1\,1\,1)/I(1\,0\,0) \approx 50$, indicating a partially ordered $L1_2$ structure (space group $Pm3m$) is preferred over the disordered A1 structure (space group $Fm3m$) at high $ScCl_3$ content. Modelling of the $I(1\,1\,1)/I(1\,0\,0)$ ratio indicates that the excess Al can be placed on the Sc sublattice to achieve the necessary quenching of ordering reflections such as (1 0 0), giving a simple $Al_3(Al_{0.5}Sc_{0.5})$ $Pm3m$ composition. By itself, this phase accounts for 79.16% of the originally added Sc atoms. At high mol% $TiCl_3$ content, we have observed a minor proportion of Ti-poor a-$Al_{1-x}Ti_x$ ($x < 0.15$) phase [20], however, inspection of Fig. 1 reveals that for the H cycled $NaAlH_4 + 0.1ScCl_3$ system, there is no discernible deviation in the 2 Å region, suggesting that the formation of a-$Al_{1-x}Sc_x$ has not occurred. Literature relating to the formation of amorphous $Al_{1-x}Sc_x$ phases is sparse, with the only known comprehensive study indicating that at <15 at.% Sc, only quasicrystalline $Al_{1-x}Sc_x$ ($x < 0.15$) phases will form from melt spun ribbons [36]. While this study by itself does not definitively rule out the possibility of a-$Al_{1-x}Sc_x$ phase formation, the lack of a deviation in the 2 Å region in our data is compelling evidence that a-$Al_{1-x}Sc_x$ phase formation is avoided at high $ScCl_3$ content. As such, the strong reduction in absorption kinetics at high $ScCl_3$ content cannot be explained by Sc-poor a-$Al_{1-x}Sc_x$ ($x < 0.15$), in contrast to the $TiCl_3$ case, where encapsulation/layering of the c-$Al_{85}Ti_{15}$ solid solution by the a-$Al_{1-x}Ti_x$ ($x < 0.15$) phase is the most plausible explanation of the decrease in absorption kinetics.

Closer inspection of our H cycled $NaAlH_4 + 0.1ScCl_3$ diffraction data in Fig. 5 reveals that while the $NaAlH_4$ proportion in the sample is small, high angle shoulders exist on every $NaAlH_4$ reflection, producing doublets. Such shoulders have not been observed previously, and are not observed for any of the other TM or RE species in our study. In addition to the 'normal' $NaAlH_4$ phase, a 'compressed' $NaAlH_4$ phase has been modelled, with unit cell dimensions $a = 4.9995(2)$ Å and $c = 11.2893(1)$ Å. The 'compressed' $NaAlH_4$ 'shoulders' are actually more intense than the 'normal' $NaAlH_4$ phase. Fig. 6(a) and (b) shows the $NaAlH_4$ unit cell dimensions for H cycled $NaAlH_4 + x TMCl_n$ for all TM and RE species in our study. The dimensions have been determined on the basis of calibration of instrumental wavelength with SRM 640c Si and SRM 660a LaB_6, with any residual zero point offset determined on the basis of the Al unit cell ($a = 4.0490$ Å) in the H cycled $NaAlH_4 + x TMCl_n$ sample. It is apparent from Fig. 6(b) that Sc appears as an anomalous case, with a significantly compressed a-axis at 10 mol% $ScCl_3$ additive level. The 'normal' $NaAlH_4$ unit cell at 10 mol% $ScCl_3$ additive level has dimensions $a = 5.0185(2)$ Å and $c = 11.3450(1)$ Å. While there is a significant spread for the c-axis with ±0.0094 Å about the average of 11.3516(1) Å (dotted line in Fig. 6(a)) for Sc–Mn and Ce, the spread about the average on the a-axis is smaller at ±0.0017 Å for all TM and RE species other than Sc. The compression of the a-axis of the 'normal' $NaAlH_4$ unit cell for H cycled $NaAlH_4 + 0.1ScCl_3$ is over double that of any other TM and RE species, at −0.0043 Å (the average of 5.0228(1) Å is also slightly biased to Sc by the 'normal' Sc a-axis), and is easily observed

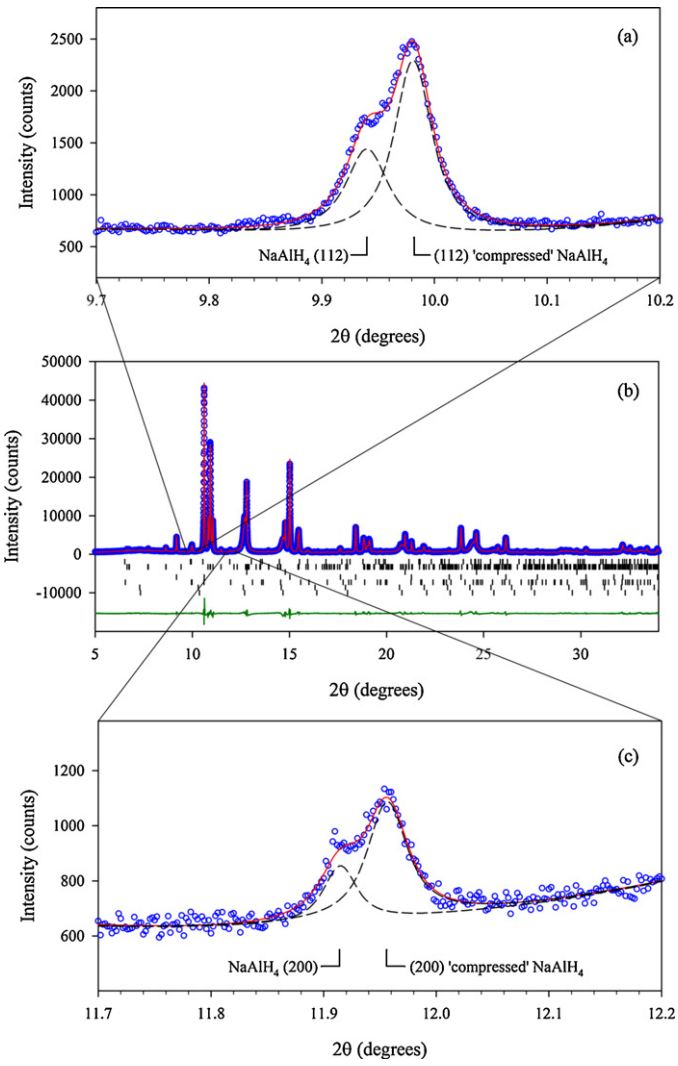

Fig. 5. Diffraction data from the twice H cycled PM $NaAlH_4 + 0.1ScCl_3$ system, showing high angle shoulders on the $NaAlH_4$ reflections for (1 1 2) in (a), and for (2 0 0) in (c). (b) Shows the total pattern fit, with reflection markers from top to bottom representing $NaAlH_4$, Na_3AlH_6, Al, NaCl, 'compressed' $NaAlH_4$, Al_3Sc, and $Al_{87.6}Sc_{12.4}$.

in Fig. 6(b) when compared to all other TM and RE species. The 'normal' and 'compressed' $NaAlH_4$ phases constitute 1.13 and 2.16 mol% of the sample respectively by QPA. The compression of the a-axis of the 'normal' $NaAlH_4$ phase in the H cycled $NaAlH_4 + 0.1ScCl_3$ sample can be understood as a mechanical contraction due to the presence of the 'compressed' $NaAlH_4$ phase, of which there is ca. twice as much. Such an inference implies an intimate connected morphology between the 'normal' and 'compressed' $NaAlH_4$ phases. While the 'slight' compression of the a-axis of the 'normal' $NaAlH_4$ phase can be understood as simple mechanical contraction, the highly significant contraction of the 'compressed' $NaAlH_4$ phase is a remarkable observation, and warrants close examination.

Fig. 6(c) and (d) compares the 'compressed' $NaAlH_4$ unit cell dimensions for H cycled $NaAlH_4 + 0.1ScCl_3$ with 'normal' H cycled $NaAlH_4 + x TMCl_n$ dimensions. The variation of the 'compressed' $NaAlH_4$ lattice parameter from the 'normal' average $NaAlH_4$ is ca. 0.5% on both the a-axis and c-axis. Such a large deviation is indicative of a change in the $NaAlH_4$ structure. Several factors must be considered before any deductions are made about what could change the $NaAlH_4$ unit cell dimensions so dramatically: (i) the diffracted intensities of the 'compressed' $NaAlH_4$ phase are

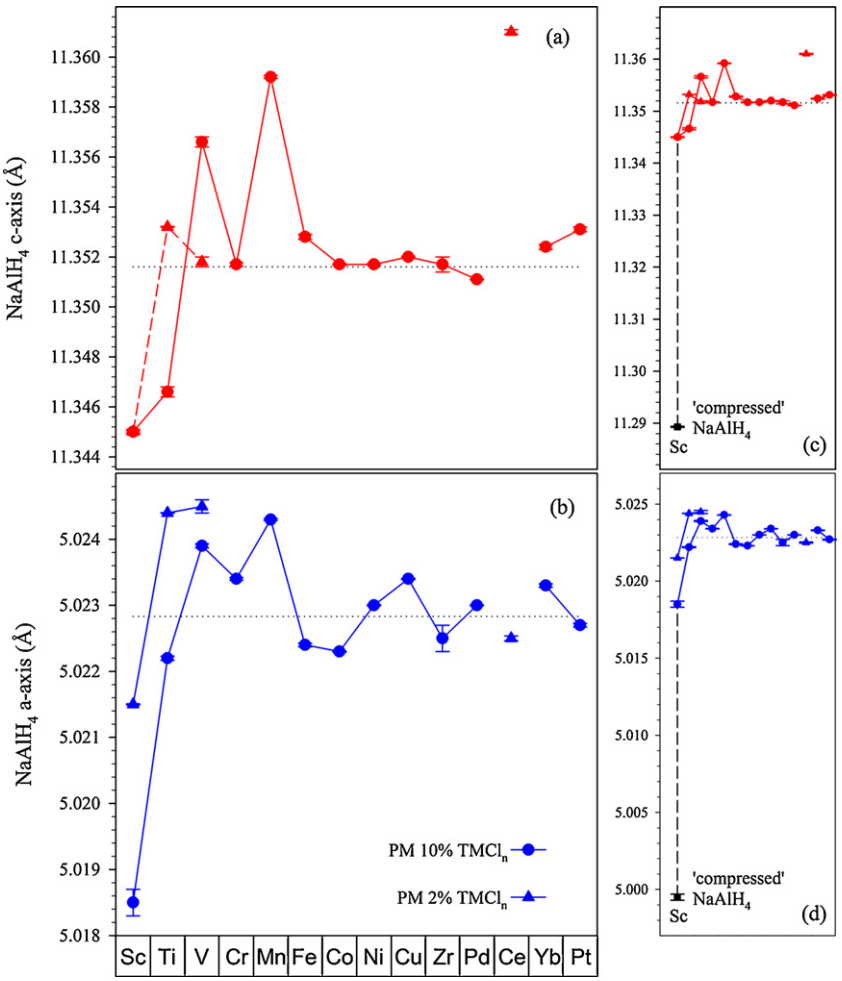

Fig. 6. Variation of the $NaAlH_4$ unit cell dimensions across the TM series for H cycled PM $NaAlH_4 + 0.1TMCl_n$. (a) Shows the variation of the *c*-axis, and (b) the *a*-axis. (c) and (d) Show the dimensions of 'compressed' $NaAlH_4$ on the *c*-axis and *a*-axis respectively for the H cycled $NaAlH_4 + 0.1ScCl_3$ system.

not able to be analysed for compositional changes at proportions in the order of 2 mol% of the sample, (ii) all NaCl expected by mechanochemical reduction is accounted for, and we do not expect Cl^- anions have substituted into the $NaAlH_4$ unit cell (the same can be said for every TM and RE species in this study), (iii) the 'compressed' $NaAlH_4$ lineshape is similar to the 'normal $NaAlH_4$ lineshape, indicating that microstructure plays no role [15], and (iv) the c-$Al_{87.6}Sc_{12.4}$ solid solution accounts for 79.16% of the originally added Sc atoms by itself, and is highly likely embedded on the powder grain surface [15], similar to the case for Ti [11,20] and V [20]. We expect that Al_3Sc will always co-exist with the c-$Al_{87.6}Sc_{12.4}$ solid solution. Including Al_3Sc in the QPA brings the total Sc atoms accounted for to 93.35% (split across $Al_{87.6}Sc_{12.4}$:Al_3Sc as 82.92%:17.08%). Without the benefit of high resolution TEM studies of the surface to identify any other $Al_{1-x}Sc_x$ phases, we presently cannot state with certainty if all originally added Sc atoms can be accounted for as $Al_{1-x}Sc_x$ or potentially ScH_x phases. Presently, the most plausible explanation is that a minor amount of Sc has penetrated the $NaAlH_4$ unit cell, and substituted either interstitially or on either the Na or Al positions. It is to be noted that such substitution must necessarily occur on the outer surface of the powder grain, where the reduction of $ScCl_3$ has occurred. If this Sc substitution hypothesis is followed to its logical conclusion, it implies that such substitution into the $NaAlH_4$ unit cell has been highly detrimental to the hydrogenation kinetics (with this sample displaying only 0.029 wt.% H/h), producing a hydrogen impermeable surface. While density functional theory (DFT) modelling has been performed on Ti substitution into the $NaAlH_4$ unit cell (with an associated compression) [37], and Sc substitution into $NaAlH_4$ [38,39], such concepts currently remain in the modelling realm, and no experimental evidence to date exists to support TM or RE substitution into $NaAlH_4$. Previous experimental studies of $TiCl_3$ enhanced $NaAlH_4$ found no variation in $NaAlH_4$ lattice parameters compared to pure $NaAlH_4$ [40,41]. In general, such models are implausible with regard to the experimentally observed H cycled $NaAlH_4 + xTMCl_n$ morphology, where TM atoms are bound within nanoscopic $Al_{1-x}TM_x$ phases embedded on the $NaAlH_4$ surface [11,15,20]. However, we note that solid solutions of similarly charged cations do exist in tetravalent complex hydrides, such as the recently discovered $Mg_xMn_{1-x}(BH_4)_2$ ($0 < x < 0.8$) system [42]. Based on a similar cation valence, we expect a charge balanced $NaAl_{1-x}Sc_xH_4$ type structure. The H cycled $NaAlH_4 + xScCl_3$ system clearly must be studied at intermediate ($0.02 < x < 0.1$) mol% $ScCl_3$ additive level, in order that a sufficient quantity of 'compressed' $NaAlH_4$ can be observed. Such a study would preferentially use neutron diffraction to ensure the highest contrast to study any modification in the intensities of the 'compressed' $NaAlD_4$ phase (likely a $NaAl_{1-x}Sc_xD_4$ composition). The use of $ScCl_3$ should be limited to 2 mol% additive level to avoid the kinetically detrimental formation of the 'compressed' $NaAlH_4$ phase.

The formation of c-$Al_{90}V_{10}$ solid solution in H cycled PM $NaAlH_4 + 0.1VCl_3$ has been discussed extensively in an earlier study [20]. c-$Al_{90}V_{10}$ is observed in a composite layered morphology, embedded within an a-$Al_{72}V_{28}$ matrix. At 2 mol% VCl_3

additive level, the c-$Al_{1-x}V_x$ solid solution indexes with an identical 4.0281(1) Å unit cell, indicating the same c-$Al_{90}V_{10}$ composition. Rietveld refinement and QPA modeling of the unknown a-$Al_{1-x}V_x$ composition in H cycled $NaAlH_4$ + 0.02VCl_3 yields an a-$Al_{90}V_{10}$ composition, with 100% of the originally added V atoms accounted for and split across c-$Al_{90}V_{10}$:a-$Al_{90}V_{10}$ as 14.73%:85.27%. For H cycled CM $NaAlH_4$ + 0.1VCl_3, the c-$Al_{1-x}V_x$ solid solution reflections are absent, and only an a-$Al_{1-x}V_x$ halo can be observed in the data. The absorption kinetics of the H cycled CM $NaAlH_4$ + 0.1VCl_3 sample are reduced to 0.0129 wt.% H/h, strongly indicating that the c-$Al_{90}V_{10}$ solid solution is the kinetically active phase. QPA of the primary a-$Al_{1-x}V_x$ halo yields an a-$Al_{83}V_{17}$ composition for the H cycled CM 10 mol% VCl_3 additive level, with 100% of the originally added V atoms accounted for. The distribution of V atoms across c-$Al_{90}V_{10}$:a-$Al_{1-x}V_x$ for both PM and CM VCl_3 at all additive levels studied are reported in Table 1. Experimentally determined unit cell dimensions of solid solutions of c-$Al_{99.4}V_{0.6}$ and c-$Al_{98.2}V_{1.8}$ are reported in [43,23] respectively. Although not observed experimentally, a metastable cubic $L1_2$ Al_3V composition has been calculated, with good agreement between several calculations [44–46], giving an average unit cell dimension of a = 3.8990 Å.

An $Al_{98.3}Zr_{1.7}$ composition is reported in [14] for re-hydrogenated PM $NaAlH_4$ + 0.04–0.1$ZrCl_4$. The $Al_{98.3}Zr_{1.7}$ unit cell dimension is 4.0731 Å, very close to the 4.0724(1) Å $Al_{1-x}Zr_x$ unit cell in our data for twice H cycled $NaAlH_4$ + 0.1$ZrCl_4$. The $Al_{98.3}Zr_{1.7}$ composition in [14] was determined based on an early report [47], and can be reassessed as a slightly Zr richer $Al_{94.5}Zr_{5.5}$ composition on the basis of the recently determined concentration dependent lattice parameters reported in [28]. The observation of a significantly Zr richer $Al_{80}Zr_{20}$ $L1_2$ structure for $NaAlH_4$ + 0.25$ZrCl_4$ in [14] is consistent with the observation of single phase $Al_{90}Zr_{10}$ which also displays intense $L1_2$ ordering reflections [48], whose structure is analysed in [10]. This suggests that Zr is analogous to Ti, and is continuously solved into Al up to 25 at.%. In our twice H cycled PM $NaAlH_4$ + 0.1$ZrCl_4$ sample, we observe $Al_{94.5}Zr_{5.5}$, metastable cubic Al_3Zr, and a minor proportion of ZrH_2. The distribution of Zr atoms across these phases is described in Table 1.

The Cr, Mn, Co and Pd $Al_{1-x}TM_x$ phases are unique, and what appear to be primary amorphous halos in the diffraction patterns in Fig. 7 are in fact extremely broad reflections from nanoscopic high symmetry bcc phases. This observation stems from the unique properties of c-$Al_{1-x}Cr_x$, c-$Al_{1-x}Mn_x$, c-$Al_{1-x}Co_x$ and c-$Al_{1-x}Pd_x$ phases to form dimensionally coherent high symmetry A2 and B2 structure types intermediate between the amorphous and quasi-crystalline state [49,50]. For twice H cycled CM $NaAlH_4$ + 0.1$CrCl_3$, we observe c-$Al_{48.2}Cr_{51.8}$ with a unit cell parameter of 3.0200(3) Å, consistent with the extrapolation of the known concentration dependent unit cell parameters in [51]. Lineshape analysis indicates the $Al_{48.2}Cr_{51.8}$ crystallites are ca. 2.72(3) nm in dimension. The distribution of Cr atoms between bcc c-$Al_{48.2}Cr_{51.8}$ and fcc c-$Al_{97.73}Cr_{2.27}$ is described in Table 1. The twice H cycled PM $NaAlH_4$ + 0.1$MnCl_2$ sample displays a c-$Al_{65.5}Mn_{34.5}$ phase with a unit cell parameter of 2.9901(1) Å, at the lower limit of the Mn solubility range of the bcc γ-AlMn phase (34.5–51.3 at.% Mn) [52]. The twice H cycled PM $NaAlH_4$ + 0.1$CoCl_2$ sample displays only a single phase of ordered B2 AlCo, with unit cell dimension 2.8919(3) Å. QPA accounts for 100% of the originally added Co atoms. Lineshape analysis indicates the AlCo crystallites are ca. 3.11(4) nm in dimension. For twice H cycled PM $NaAlH_4$ + 0.1$PdCl_2$, we observe β-AlPd with a unit cell dimension of 3.0123(1) Å. This is lower than the reported value of 3.0490 Å in [53]. The solubility range of Pd in β-AlPd is wide, 44–57 at.% [54], and as such, we expect a concentration dependent range for the unit cell parameter, similar to Cr and Mn. To our knowledge, this concentration dependence has not yet been reported, and we have currently modeled the phase as a

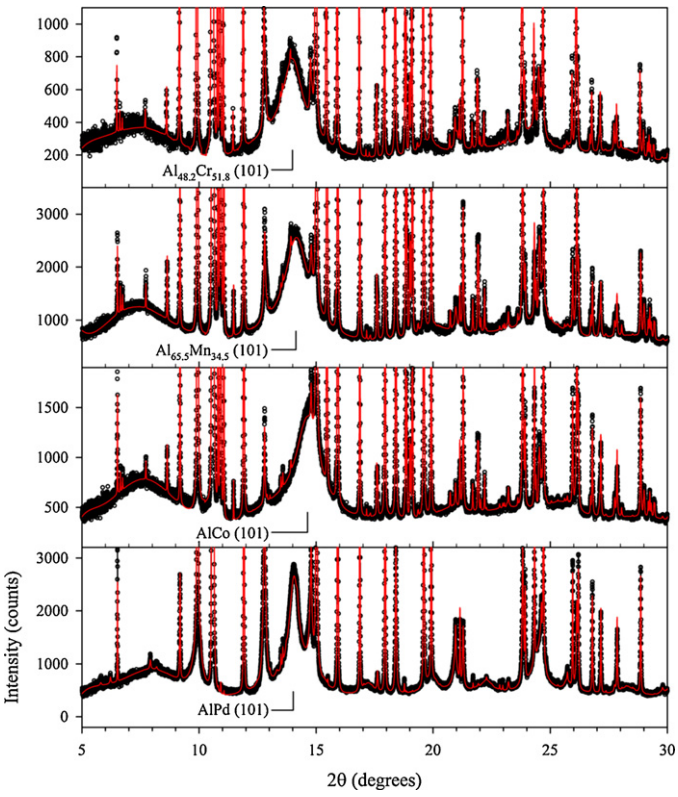

Fig. 7. Rietveld calculated fits to twice H cycled $NaAlH_4$ + 0.1$TMCl_n$ (TM = Cr, Mn, Co and Pd) samples. The strongest (1 0 1) reflection of the A2 (Cr, Mn) and B2 (Co, Pd) structures is evident as a very broad peak, with maxima centred at 13.98°, 14.14°, 14.63° and 14.02° 2θ, respectively. The earlier broad peak at ca. 8° 2θ is the primary amorphous halo from the quartz capillary.

1:1 composition. In this fashion, 42.4% of Pd atoms are accounted for in the B2 AlPd structure type. We also observe an fcc $Al_{1-x}Pd_x$ solid solution that presents with high d-spacing shoulders on Al reflections (see Fig. 2). The solubility limit of Pd in Al has been reported as $Al_{90}Pd_{10}$ in [29]. No concentration dependent unit cell dimensions have been reported for $Al_{1-x}Pd_x$ (x < 0.25), and we have modeled the phase at the limiting composition of $Al_{90}Pd_{10}$. The distribution of Pd atoms across all c-$Al_{1-x}Pd_x$ phases is described in Table 1. Fig. 7 compares the Rietveld fits to the synchrotron X-ray data for H cycled PM $NaAlH_4$ + 0.1$TMCl_n$ (TM = Cr, Mn, Co and Pd) samples with the calculated intensity contribution of the A2 (Cr, Mn) and B2 (Co, Pd) type structures shown. The maxima of the main broad (1 0 1) reflection is at ca. 13.98°, 14.14°, 14.63° and 14.02° 2θ respectively for Cr, Mn, Co and Pd. Reflections from the B2 type structure other than (1 0 1) are more easily observed for AlPd than AlCo as Pd has a much larger X-ray scattering factor. It is clear that a wide variety of TM poor to rich $Al_{1-x}TM_x$ phases are observed across the TM series for the H cycled PM $NaAlH_4$ + 0.1$TMCl_n$ system, and the correct identification of them is challenging, particularly when they are considerably small in dimension, <5 nm, resulting in extremely broad reflections in diffraction data.

For the later TM atoms Ni, Cu, Pd and Pt in H cycled PM $NaAlH_4$ + 0.1$TMCl_n$ samples, we do not typically observe crystalline $Al_{1-x}TM_x$ solid solutions, rather, numerous ordered c-$Al_{1-x}TM_x$ phases appear in the diffraction data, and a wide range of Al:TM compositions are present. Fig. 8 shows the Rietveld refinement of synchrotron X-ray data for the H cycled PM $NaAlH_4$ + 0.1$NiCl_2$ sample, with the inset showing the complex low angle reflection overlap which can occur when numerous c-$Al_{1-x}TM_x$ phases are present. We observe five c-$Al_{1-x}Ni_x$ phases, four c-$Al_{1-x}Cu_x$ phases, six c-$Al_{1-x}Pd_x$ phases, and eleven c-$Al_{1-x}Pt_x$ phases. The Pd and Pt

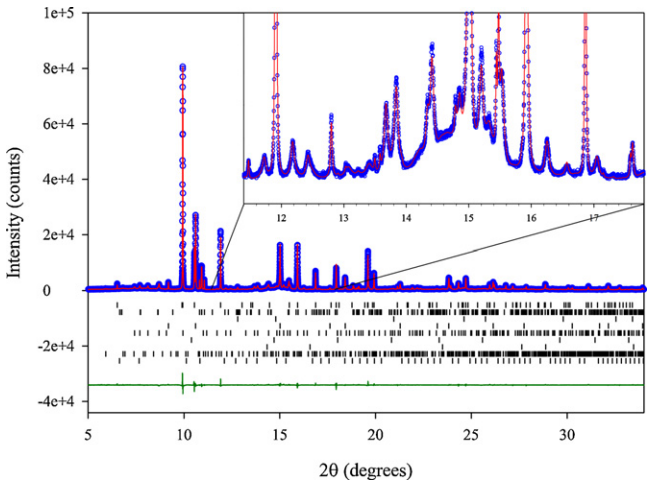

Fig. 8. Total pattern fit to twice H cycled $NaAlH_4 + 0.1NiCl_2$. Reflection markers from top to bottom represent $NaAlH_4$, Na_3AlH_6, Al, NaCl, Al_3Ni, AlNi, $Ni_{86}Al_{14}$, Al_9Ni_2, and Al_4Ni_3. The inset figure from 11.4 to 17.8° 2θ shows some of the complex low angle reflection overlap from numerous $Al_{1-x}Ni_x$ phases. Such complex overlap is typically observed in the Ni, Cu, Pd and Pt systems.

diffraction patterns are particularly complex and challenging to fit. Even with eleven $Al_{1-x}Pt_x$ phases fitted, there still remain some unfitted intensities for the H cycled PM $NaAlH_4 + 0.1PtCl_4$ data. This is a direct reflection of the complexity of the Al–Pt binary phase diagram [55], which remains to be completely described. Although Cu, Pd and Pt are kinetically poor with very low H storage capacity (particularly Pt, which has near zero capacity due to the heavy consumption of Al by the high number of $Al_{1-x}Pt_x$ phases), they remain of interest in terms of why the noble metals are not useful hydrogenation catalysts for $NaAlH_4$. The obvious inference is that the excellent molecular H_2 dissociation/recombination capability of the noble metals is removed when they form binary $Al_{1-x}TM_x$ phases, and new $Al_{1-x}TM_x$ surfaces are created. The QPA distribution of Ni, Cu, Pd and Pt atoms in their respective $Al_{1-x}TM_x$ phases is described in Table 1. We note that the manufacturer supplied $ZrCl_4$, $PdCl_2$ and $PtCl_4$ do not conform to any of the known $TM_{1-x}Cl_x$ (TM = Zr, Pd and Pt) structure types, however, $ZrCl_4$ and $PdCl_2$ produce the expected amount of NaCl after mechanochemical reduction. However, $PtCl_4$ does not produce the expected NaCl quantity. With unfitted intensities, the twice H cycled $NaAlH_4 + 0.1PtCl_4$ sample remains as the only sample we have not been able to account for 100% of the originally added TM atoms. On the basis of the amount of NaCl produced and assuming a 1:4 Pt:Cl ratio, we find ca. 65% of the originally added Pt atoms accounted for, and analysis of the complex diffraction data from the $NaAlH_4 + 0.1PtCl_4$ sample must be regarded as a work in progress.

We have also observed two new $Al_{1-x}M_x$ phases (M = TM and RE) in our twice H cycled CM $NaAlH_4 + 0.1MCl_3$ samples. Diffraction data from the twice H cycled CM $NaAlH_4 + 0.1FeCl_3$ sample displays a large cubic primitive unit cell with dimension $a = 6.8731(1)$ Å, for which we have not yet finalised a structure. The intensities in the synchrotron X-ray data from this unknown phase are very similar to the new bcc Al_2Ce phase discovered in [7], and as such, we expect a similar Al_2Fe composition. The twice H cycled CM $NaAlH_4 + 0.1YbCl_3$ also proves interesting. No amorphous phase is formed in the $NaAlH_4 + 0.1YbCl_3$ system, suggesting the rare earths (RE) behave like the later transition metals, Cu, Pt, etc. and form only c-$Al_{1-x}Yb_x$ phases, even though a-$Al_{1-x}Yb_x$ and a-$Al_{1-x}RE_x$ phases are well observed and studied [56–58]. Instead we observe a new intermetallic phase not previously observed in the equilibrium Al–Yb phase diagram, Al_2Yb ($P4/mmm$, $a = 3.6403(1)$ Å, $c = 8.3574(3)$ Å, Yb (0, 0, 0), Al (½, ½, 0.2748(3))) and YbH_3 with coherence length ca. 10.43(8) nm. Al_2Yb typically forms in a stable cubic Laves C15 A_2B structure type [59]. This indicates the cryo mill is an excellent tool for producing nanoscopic non-equilibrium $Al_{1-x}M_x$ phases (M = TM and RE) phases in H cycled MCl_n enhanced $NaAlH_4$.

Table 2
$Al_{1-x}Ti_x$ phases observed in the PM and H cycled $NaAlH_4 + xTiCl_3$ ($0.02 < x < 0.15$) system for all milling/pressure/temperature conditions utilised in our previous studies [10,11,20,60].

$TiCl_3$ (i)	$TiCl_3$ (ii)	$TiCl_3$ (iii)	$TiCl_3$ (iv)
$Al_{86}Ti_{14}$ (PM 10 mol%) Isochronal Annealing 2 °c/min [10]	$Al_{91}Ti_9$ $Al_{87.5}Ti_{12.5}$ $Al_{80}Ti_{20}$ (PM 48 h 10 mol%) [10]	$Al_{89}Ti_{11}$ $Al_{82}Ti_{18}$ Al_3Ti Al_2Ti (PM 2 mol%) ×1 H cycle [11]	c-$Al_{85}Ti_{15}$ c-Al_3Ti a-$Al_{92}Ti_8$ c-TiH_{2-x} [60] a-TiH_{2-x} [60] (PM 10 mol%) ×5 H cycle [20]
$Al_{88}Ti_{12}$ (PM 10 mol%) Isothermal annealing 140 °C for 12 h [10]	c-$Al_{85}Ti_{15}$ c-Al_3Ti a-$Al_{92}Ti_8$ (PM 10, 15 mol%) ×2 H cycle [20] $Al_{85}Ti_{15}$ Al_3Ti (PM 5 mol%) ×2 H cycle [11]	$Al_{85}Ti_{15}$ Al_3Ti (PM 2 mol%) ×10 H cycle [11]	c-$Al_{84}Ti_{16}$ a-$Al_{86.5}Ti_{13.5}$ (CM 10 mol%) ×2 H cycle [20]

As a reference, Table 2 provides all $Al_{1-x}Ti_x$ phases we observe for the PM and H cycled $NaAlH_4 + xTiCl_3$ ($0.02 < x < 0.15$) system for all milling/pressure/temperature conditions utilised in our previous studies [10,11,20,60]. Inspection of Tables 1 and 2 shows that across the TM series, the presence of amorphous $Al_{1-x}TM_x$ phases is limited to the early transition metals Ti, V, and Fe. For Ti and V, the a-$Al_{1-x}TM_x$ phases co-exist nanoscopically on the $NaAlH_4$ surface in a composite morphology with small ca. 4–25 nm fcc c-$Al_{1-x}TM_x$ solid solutions. H cycled PM $NaAlH_4 + 0.1FeCl_3$ is a unique case, where all Fe atoms are consumed within the a-$Al_{1-x}Fe_x$ phase. The Cr, Mn, Co and Pd $Al_{1-x}TM_x$ phases typically contain the majority of TM atoms in small ca. 3 nm bcc (A2 and B2) $Al_{1-x}TM_x$ phases. For the later TM atoms, Ni, Cu, Pd and Pt, some of the $Al_{1-x}TM_x$ phases display considerably sharper reflections, such as Al_2Cu (>50 nm coherence length), and the number of c-$Al_{1-x}TM_x$ phases becomes larger, with considerably more complex diffraction patterns. Aside from the Ni case, the Cu, Pd and Pt based samples are kinetically and H storage irrelevant.

With moderate H cycling of the $TiCl_3$ enhanced $NaAlH_4$ system, long term isothermal ageing with H cycling shows a steady conversion of c-$Al_{85}Ti_{15}$ into c-Al_3Ti [11]. Such behavior is analogous to the well-studied Al–Sc system, where high temperature ageing of dilute crystalline $Al_{1-x}Sc_x$ solid solutions (typically 0.06–0.2 at.%) nucleates fine nanoscale precipitates of ordered $L1_2$ Al_3Sc [35]. Such behavior suggests that independent of TM type, short term high temperature ageing (>300 °C) can be observed at lower H cycling temperatures such as ca. 140–150 °C, over the course of ca. 100 H cycles, and that eventually, the starting c-$Al_{1-x}TM_x$ phase (if different to the most stable phase) will be fully converted to the most thermodynamically stable phase in the Al–TM phase diagram. This is possible as Al can be both removed and added to the starting c-$Al_{1-x}TM_x$ phase as necessary to produce the most stable c-$Al_{1-x}TM_x$ phase, at the addition or expense of Al from the $NaAlH_4$, Na_3AlH_6 or Al phases. As an example, β-AlPd initially appears as a minor Pd containing phase (ca. 42% of all Pd atoms) during the early H cycles, however, it is the most stable phase in the Al–Pd phase diagram [53], and we should expect it to consume all Pd atoms with long term H cycling. Diffraction data from MCl_n enhanced $NaAlH_4$

typically does not exist beyond 100 H cycles, and as such, it is presently not possible to confirm for any TM or RE species if the most thermodynamically stable $Al_{1-x}TM_x$ or $Al_{1-x}RE_x$ phases do eventually consume all of the added TM or RE atoms. As the observed $Al_{1-x}M_x$ phases can exist on a very fine nanoscopic scale <5 nm, it is also plausible that a quasi-equilibrium state is reached where many $Al_{1-x}M_x$ compositions may exist together for the same M atom.

4. Conclusion

Across the H cycled PM $NaAlH_4 + 0.1TMCl_n$ series, we observe a wide range of nanoscopically dimensioned a-$Al_{1-x}TM_x$ and c-$Al_{1-x}TM_x$ phases, Sc–V ca. 4–25 nm, Cr, Mn, Co <5 nm, Fe 5–15 nm, Ni, Cu <50 nm. In general, 100% of the originally added TM atoms for $NaAlH_4 + xTMCl_n$ can be accounted for by QPA as a combination of c-$Al_{1-x}TM_x$ and/or a-$Al_{1-x}TM_x$ phases. We expect that independent of TM type, the most stable c-$Al_{1-x}TM_x$ phase will form/increase in proportion with long term H cycling. Although we have not obtained TEM size distributions for any TM atoms other than Ti and Ni, and high resolution TEM images for Ti, V and Fe [20], we believe that a similar mechanochemical reduction reaction occurs during ball milling for all TM species, and that all $Al_{1-x}TM_x$ phases which form/crystallise from the reduction by-products during milling and subsequent H cycling are similarly well distributed as small isolated nanoscopic crystals/amorphous phases, embedded on the $NaAlH_4$ surface. The proportion and composition of $Al_{1-x}TM_x$ phases formed is strongly dependent on mol% $TMCl_n$ and H cycling conditions. The formation of a highly 'compressed' $NaAlH_4$ phase in the H cycled PM $NaAlH_4 + 0.1ScCl_3$ system appears to be unique to Sc only, and its presence appears to be highly detrimental to hydrogenation kinetics.

Acknowledgements

This work was supported by the Synchrotron Program of the Research Council of Norway. MPP thanks the staff of the Swiss-Norwegian Beam Line for providing experimental assistance and logistics during long-term attachments.

References

[1] B. Bogdanovic, M. Felderhoff, A. Pommerin, F. Schuth, N. Spielkamp, Adv. Mater. 18 (2006) 1198–1201.
[2] T. Wang, J. Wang, A.D. Ebner, J.A. Ritter, Alloys Compd. J. 450 (2008) 293–300.
[3] B. Bogdanovic, M. Felderhoff, A. Pommerin, F. Schuth, N. Spielkamp, A. Stark, Alloys Compd. J. 471 (2009) 383–386.
[4] M.H.W. Verkuijlen, P.J.M. van Bentum, O. Zabara, M. Fichtner, A.P.M. Kentgens, J. Phys. Chem. C 115 (2011) 13100–13106.
[5] A. Leon, J. Rothe, K. Chlopek, O. Zabara, M. Fichtner, Phys. Chem. Chem. Phys. 11 (2009) 8829–8834.
[6] X. Fan, X. Xiao, L. Chen, S. Li, Q. Wang, Alloys Compd. J. 509 (2010) S750–S753.
[7] M.P. Pitt, M. Paskevicius, C.J. Webb, M.H. Sorby, S. Delleda, T.R. Jensen, B.C. Hauback, C.E. Buckley, E.M. Gray, Int. J. Hydrogen Energy 36 (2011) 8403–8411.
[8] D. Anton, J. Alloys Compd. 356–357 (2003) 400–404.
[9] T. Sun, B. Zhou, H. Wang, M. Zhu, Int. J. Hydrogen Energy 33 (2008) 2260–2267.
[10] M.P. Pitt, P.E. Vullum, M.H. Sorby, M.P. Sulic, C.M. Jensen, J.C. Walmsley, R. Holmestad, B.C. Hauback, Acta Mater. 56 (2008) 4691–4701.
[11] M.P. Pitt, P.E. Vullum, M.H. Sorby, H. Emerich, M. Paskevicius, C.E. Buckley, E.M. Gray, J.C. Walmsley, R. Holmestad, B.C. Hauback, submitted for publication.
[12] C. Rongeat, N. Scheerbaum, L. Schultz, O. Gutfleisch, Acta Mater. 59 (2011) 1725–1733.
[13] Y. Suttisawat, V. Jannatisin, P. Rangsunvigit, B. Kitiyanan, N. Muangsin, S. Kulprathipanja, Power Sources J. 163 (2007) 997–1002.
[14] C. Weidenthaler, A. Pommerin, M. Felderhoff, B. Bogdanovic, F. Schuth, Phys. Chem. Chem. Phys. 5 (2003) 5149–5153.
[15] M.P. Pitt, P.E. Vullum, M.H. Sorby, D. Blanchard, M.P. Sulic, H. Emerich, M. Paskevicius, C.E. Buckley, J.C. Walmsley, R. Holmestad, B.C. Hauback, Alloys Compd. J. 513 (2012) 597–605.
[16] M.P. Pitt, P.E. Vullum, M.H. Sorby, D. Blanchard, M.P. Sulic, H. Emerich, M. Paskevicius, C.E. Buckley, J.C. Walmsley, R. Holmestad, B.C. Hauback, Alloys Compd. J. 514 (2012) 163–169.
[17] K.G. McLennan, E.M. Gray, Measur. Sci. Technol. 15 (2004) 211–215.
[18] E.M. Gray, Reliably measuring hydrogen uptake in storage materials, in: G. Walker (Ed.), Solid-State Hydrogen Storage: Materials and Chemistry, Woodhead Publishing, London, 2008.
[19] B.A. Hunter, Commun. Powder Diffract. Newslett. 20 (1998) 21.
[20] M.P. Pitt, P.E. Vullum, M.H. Sorby, H. Emerich, M. Paskevicius, C.E. Buckley, E.M. Gray, J.C. Walmsley, R. Holmestad, B.C. Hauback, J. Alloys Compd. (2012), doi:10.1016/j.jallcom.2012.01.062.
[21] J. Royset, N. Ryum, Int. Mater. Rev. 50 (2005) 19–44.
[22] A. Tonejc, A. Bonefacic, Scr. Metall. 3 (1969) 145–148.
[23] M. Moss, Acta Metall. 16 (1968) 321–326.
[24] L. Bendersky, R.J. Schaefer, F.S. Biancaniello, D. Shectman, J. Mater. Sci. 21 (1986) 1889–1896.
[25] M.K. Banerjee, J. Mater. Sci. 32 (1997) 6645–6651.
[26] C.A. Majid, Nucl. Instrum. Methods Phys. Res. Sect. B 149 (1999) 433–444.
[27] A. Shukla, A.D. Pelton, J. Phase Equilib. Diffus. 30 (2009) 28–39.
[28] T. Tsuda, C.L. Hussey, G.R. Stafford, O. Kongstein, Electrochem. Soc. J. 151 (2004) C447–C454.
[29] G.V.S. Sastry, C. Suryanarayana, Mater. Sci. Eng. 47 (1981) 193–208.
[30] M. Li, C. Li, F. Wang, W. Zhang, Intermetallics 14 (2006) 39–46.
[31] M. Ocko, E. Babic, V. Zlatic, Solid State Commun. 18 (1976) 705–708.
[32] J.F. Cannon, H.T. Hall, J. Less-Comm. Met. 40 (1975) 313–328.
[33] M. Schoenitz, Z. Xiaoying, E.L. Dreizin, J. Meta NanoCryst. Mater. 20–21 (2004) 455–461.
[34] J.L. Murray, J. Phase Equilib. 19 (1998) 380–384.
[35] E.A. Marquis, D.N. Seidman, Acta Mater. 49 (2001) 1909–1919.
[36] A. Slipenyuk, D. Lotsko, Y. Milman, M. Yefimov, M. Danylenko, Influence of scandium on amorphization of aluminum alloys, in: O.N. Senkov, D.B. Miracle, S.A. Firstov (Eds.), Proceedings of the NATO Advanced Research Workshop: Metallic Materials with High Structural Efficiency, Springer, Kyiv, Ukraine, 2003, pp. 119–124.
[37] O.M. Lovvik, S.M. Opalka, Phys. Rev. B: Condens. Matter Mater. Phys. 71 (2005) 054103.
[38] J. Liu, Q. Ge, J. Alloys Compd. 446–447 (2007) 267–270.
[39] H. Wang, A. Tezuka, H. Ogawa, T. Ikeshoji, Phys. Rev. B: Condens. Matter Mater. Phys. 83 (2011) 045112.
[40] H.W. Brinks, C.M. Jensen, S.S. Srinivasan, B.C. hauback, D. Blanchard, K. Murphy, J. Alloys Compd. 376 (2004) 215–221.
[41] H.W. Brinks, B.C. Hauback, S.S. Srinivasan, C.M. Jensen, Phys. Chem. J. B 109 (2005) 15780–15785.
[42] R. Cerny, N. Penin, V. D'Anna, H. Hagemann, E. Durand, J. Ruzicka, Acta Mater. 59 (2011) 5171–5180.
[43] N.I. Varich, L.M. Burov, K.Y. Kolesnichenko, A.P. Maksimenko, Phys. Met. Metall. 15 (1963) 111–113.
[44] M. Krajci, J. Hafner, J. Phys.: Condens. Matter 14 (2002) 1865–1879.
[45] M. Jahnatek, M. Krajci, J. Hafner, Phys. Rev. B: Condens. Matter Mater. Phys. 71 (2005) 024101.
[46] R. Boulechfar, S. Ghemid, H. Meradji, B. Bouhafs, Physica B 405 (2010) 4045–4050.
[47] T. Ohashi, R. Ichikawa, Metall. Trans. 3 (1972) 2300–2302.
[48] R.B. Schwarz, P.B. Desch, S.R. Srinivasan, in: J.J. deBarbadillo, F.H. Fores, R. Schwarz (Eds.), Proceedings of the 2nd International Conference on Structural Applications of Mechanical Alloying, ASM, Ohio, 1993, p. 227.
[49] K. Chattopadhyay, S. Lele, N. Thangaraj, S. Ranganathan, Acta Metall. 35 (1987) 727–733.
[50] Y. Weisskopf, S. Burkardt, M. Erbudak, J.-N. Longchamp, Surf. Sci. 601 (2007) 544–551.
[51] M. Ellner, I. Park, Metall. Mater. Trans. A 33 (2002) 3591–3595.
[52] V. Raghavan, J. Phase Equilib. Diffus. 26 (2005) 256–261.
[53] M. Ellner, U. Kattner, B. Predel, J. Less-Comm. Met. 87 (1982) 117–133.
[54] H. Okamoto, J. Phase Equilib. Diffus. 24 (2003) 196.
[55] K. Wu, Z. Jin, J. Phase Equilib. Diffus. 21 (2000) 221–226.
[56] J.R. Ding, D.Z. Che, H.B. Zhang, K. Tao, B.X. Liu, Appl. Phys. Lett. 60 (1992) 944–946.
[57] K.F. Liang, P. Grutter, J. Appl. Phys. 92 (2002) 6895–6899.
[58] R. Bacewicz, J. Antonowicz, Scr. Mater. 54 (2006) 1187–1191.
[59] M.C. Gao, A.D. Rollet, M. Widom, Phys. Rev. B: Condens. Matter Mater. Phys. 75 (2007) 174120.
[60] P.E. Vullum, M. Pitt, J. Walmsley, B. Hauback, R. Holmestad, Appl. Phys. A: Mater. Sci. Process. 94 (2009) 787–793.